ACS APPLIED MATERIALS & INTERFACES

www.acsami.org

Research Article

Supramolecular Peptide Nanofiber/PLGA Nanocomposites for Enhancing Pulmonary Drug Delivery

Uday Chintapula,[‖] Su Yang,[‖] Trinh Nguyen, Yang Li, Justyn Jaworski, He Dong,* and Kytai T. Nguyen*

Cite This: https://doi.org/10.1021/acsami.2c15204

Read Online

ACCESS | Metrics & More | Article Recommendations | Supporting Information

ABSTRACT: Effective drug delivery to pulmonary sites will benefit from the design and synthesis of novel drug delivery systems that can overcome various tissue and cellular barriers. Cell penetrating peptides (CPPs) have shown promise for intracellular delivery of various imaging probes and therapeutics. Although CPPs improve delivery efficacy to a certain extent, they still lack the scope of engineering to improve the payload capacity and protect the payload from the physiological environment in drug delivery applications. Inspired by recent advances of CPPs and CPP-functionalized nanoparticles, in this work, we demonstrate a novel nanocomposite consisting of fiber-forming supramolecular CPPs that are coated onto polylactic-glycolic acid (PLGA) nanoparticles to enhance pulmonary drug delivery. These nanocomposites show a threefold higher intracellular delivery of nanoparticles in various cells including primary lung epithelial cells, macrophages, and a 10-fold increase in endothelial cells compared to naked PLGA nanoparticles or a twofold increase compared to nanoparticles modified with traditional monomeric CPPs. Cell uptake studies suggest that nanocomposites likely enter cells through mixed macropinocytosis and passive energy-independent mechanisms, which is followed by endosomal escape within 24 h. Nanocomposites also showed potent mucus permeation. More importantly, freeze-drying and nebulizing formulated nanocomposite powder did not affect their physiochemical and biological activity, which further highlights the translative potential for use as a stable drug carrier for pulmonary drug delivery. We expect nanocomposites based on peptide nanofibers, and PLGA nanoparticles can be custom designed to encapsulate and deliver a wide range of therapeutics including nucleic acids, proteins, and small-molecule drugs when employed in inhalable systems to treat various pulmonary diseases.

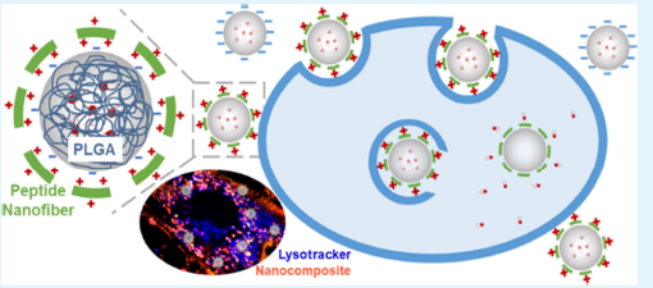

KEYWORDS: *nanocomposites, peptide self-assembly, nanofiber, PLGA nanoparticles, pulmonary delivery, endosomal escape*

1. INTRODUCTION

Nanoparticles (NPs) in the range of 1−1,000 nm with high-surface-area-to-volume ratio are being employed to deliver drugs and other therapeutics. Drug encapsulating NPs have been reported to increase the drug bioavailability and drug release in targeted tissues.[1] This, in particular, is highly beneficial to reduce the dosing frequency, improving patient compliance.[2] Commonly used NPs include polymer-based, dendrimers, liposomes, metal-based, and inorganic particles such as silica, among others. Although NPs are capable of entering cells through different endocytosis mechanisms, there is often an issue of tuning the number of NPs needed to exert a therapeutic effect.[3,4] Engineering strategies improving the uptake of NPs can have a profound effect on drug delivery toward diseased cells including infected, senescent, cancerous, and other abnormalities where an altered uptake ability or even a reduced uptake ability was seen as previously reported.[5−7]

Cell penetrating peptides (CPPs) have gained interest in the field of bioengineering given their unique ability to cross the cell membrane for intracellular drug delivery.[8,9] NPs modified with CPPs have been reported for increasing internalization in cells for various applications including targeting and imaging of cancer.[10−13] NPs are modified with CPPs by two major strategies including electrostatic interaction and covalent crosslinking such as click chemistry. Among CPPs, cationic CPPs such as the transactivator protein (Tat) of human deficiency virus (HIV) are the most frequently used for modifying NPs.[10] Arginine-rich peptides have also been used to modify NPs; for instance, Boussoufi et al.[14] directly cross-linked covalently the peptide thiol group to the surface of gold NPs for cancer therapy. In another study, polylactic-glycolic acid (PLGA) NPs were decorated with tumor-homing and penetrating peptide-F3 via amine-reactive crosslinker chemistry forming a covalent bond between the peptide and ester-activated crosslinkers on the surface of NPs and applied for

Received: August 24, 2022
Accepted: November 22, 2022

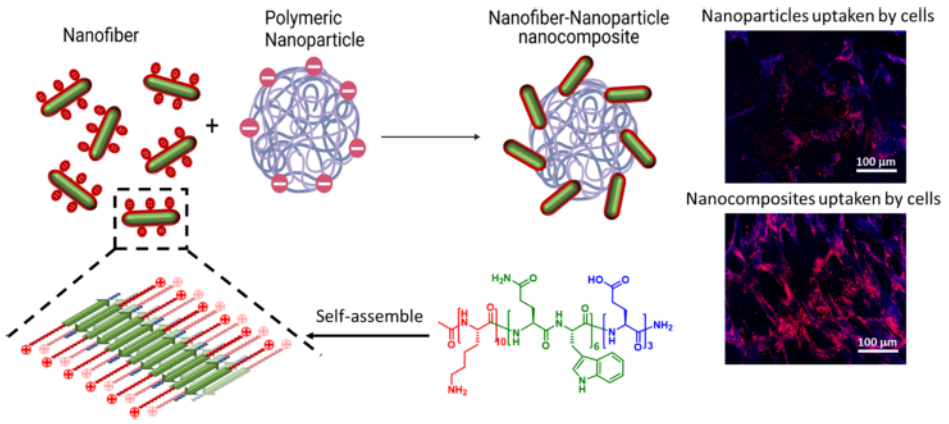

Figure 1. Overview of NC synthesis where peptides are self-assembled into NFs and electrostatically coated onto polymeric NPs to form NCs. Confocal images on the right show enhanced uptake of NPs and NCs in primary alveolar type I epithelial cells labeled with Rhodamine B dyes.

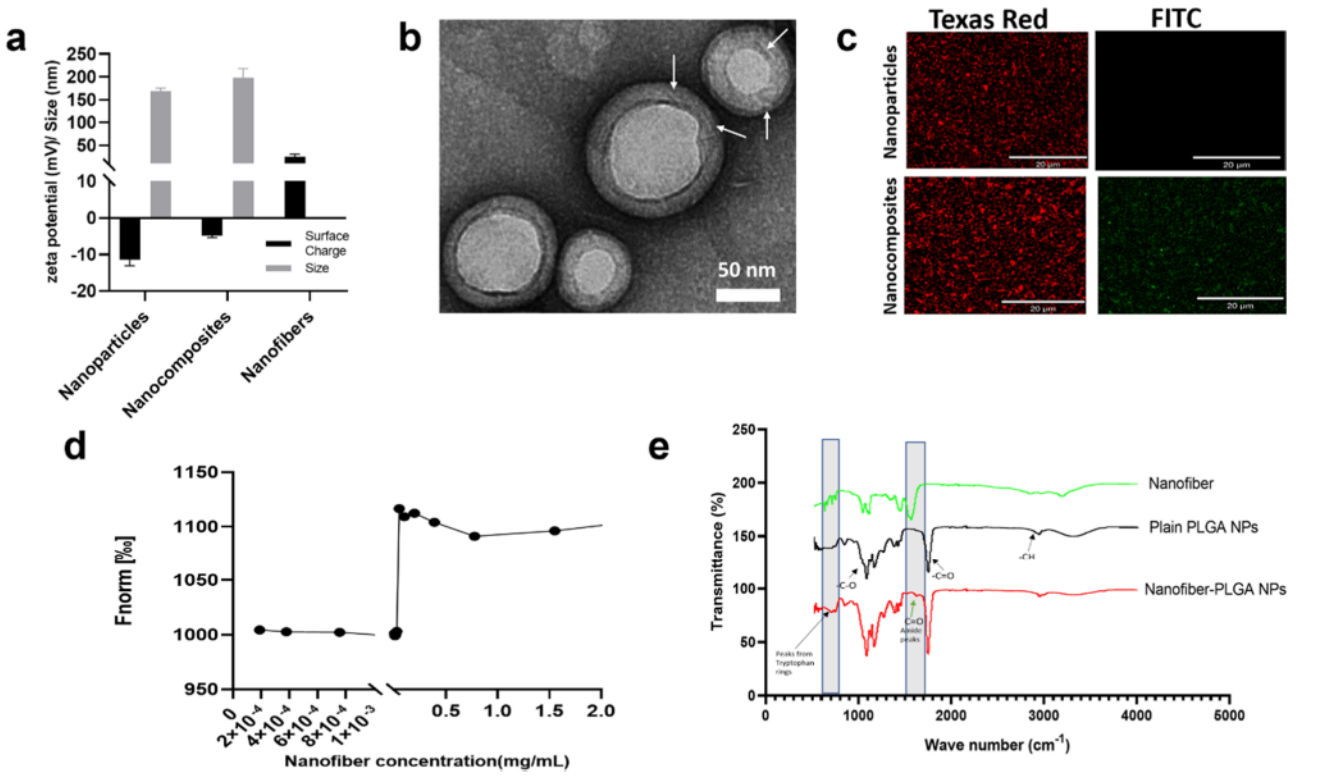

Figure 2. Characterization of NCs. (a) DLS measurements of NPs and NCs comprised NF-coated PLGA NPs showing a slight increase in size along with a reduction in charge due to a positively charged NF coating. (b) TEM image of NCs with white arrows pointing to the NFs attached to the NPs. (c) FITC-labeled NFs were coated with NPs loaded with rhodamine dye. NPs alone did not have any fluorescence in the FITC channel (green), whereas fluorescence from FITC-labeled NFs coated onto PLGA NPs can be seen in the bottom right channel (scale 20 μm). (d) Binding kinetics using thermophoresis showed increasing the concentration of NFs reduced the movement of Rhodamine B-labeled NPs (fixed concentrations) showing the effect of binding of NFs onto NPs. (e) FTIR spectra of NF-coated NPs show amide I peaks (green arrow) at 1640 cm-1 from peptides of NFs along with peaks of out of plane (C−H) bending from tryptophan rings seen at 750 cm^{-1} (black arrow).

theragnostic purposes for cancer treatment.[15] The F3-peptide coating on NPs enhanced cell association and preferential targeting to the tumor site, enabling a multimodal therapy for cancer treatment. Similarly, dual peptides of CPP Tat and antagonist G peptide were conjugated onto polymer PLGA NPs with the use of 1-ethyl-3-(3-dimethylaminopropyl)-carbodiimide−*N*-hydroxysuccinimide click chemistry, showing the ability to accommodate a multifunctional peptide coating of NPs.[16] The dual peptide coating showed lower half maximal inhibitory concentration (IC_{50}) in killing lung cancer cells compared to a single peptide modification of NPs.[16] Overall, different studies suggest that peptide modification can improve the targeting and therapeutic efficacy of NPs, thus showing a great potential for developing more efficient drug delivery systems.

Most natural and synthetic CPPs are active in the monomeric form, leading to lower binding affinity toward NPs and rapid enzymatic degradation. As a result, high concentrations of CPPs are needed to either covalently or noncovalently attach onto NPs, which in turn may cause high cytotoxicity. To address these issues, peptide self-assembly offers an effective method to generate supramolecular

https://doi.org/10.1021/acsami.2c15204
ACS Appl. Mater. Interfaces XXXX, XXX, XXX−XXX

nanomaterials with improved stability, dynamic nanostructure, and biological activity. In particular, the high aspect ratio peptide nanofibers (NFs) showed good in vivo stability and have been extensively studied as functional scaffolds and nanocarriers for a variety of in vivo biomedical applications.[17−31] Recently, a new family of supramolecular CPPs that form nanostructured fibers reported by the Yang and Dong group[32] showed potent cell penetrating activity, greatly reduced cytotoxicity, and improved proteolytic stability.[32−37] Herein, we develop a novel nanocomposite (NCs) combining these CPP nanofibers (NFs) with biodegradable PLGA NPs for enhanced pulmonary drug delivery (Figure 1). Our NFs bind to PLGA NPs electrostatically to form NCs and enhance the uptake ability of NPs with payloads for intracellular drug delivery.

2. RESULTS AND DISCUSSION

2.1. Synthesis and Characterization of NCs. The synthesis and formulation of NCs involves conjugation of oppositely charged PLGA NPs (negatively charged) and peptide NFs (positively charged). As shown in Figure 1, the NFs are composed of peptides with a primary sequence of $K_{10}(QW)_6E_3$ in which the subscript refers to the number of repeating units of each domain. All peptides were synthesized on the solid phase and characterized by matrix-assisted laser desorption/ionization-time of flight (MALDI-TOF) (Figure S1). As shown in our previous studies, $K_{10}(QW)_6E_3$ can self-assemble into NFs in which the charged residues are displayed on the exterior of the fiber surface.[32] Due to the excess of the positive charges distributed along the long fiber axis, these NFs demonstrated exceptional cell penetrating activity. In this study, we will employ these NFs that undergo charge complexation with biodegradable PLGA NPs composition for drug delivery application to develop our novel pulmonary drug delivery system.[38] PLGA NPs have greater advantages as drug delivery vehicles due to their high surface areas and hold the capability to deliver high concentrations of drugs with a prolonged release in the lungs while avoiding systemic overdose from circulation through intravenous delivery.[39] The PLGA NPs targeted in this study have a size of ∼200 nm (Figure 2a), which is suitable for lower respiratory tract delivery avoiding exhalation and upper respiratory tract accumulation.[40] Ohashi et al. have formulated rifampicin-loaded PLGA NPs of ∼213 nm in diameter and successfully delivered them to alveolar macrophages, while micron-meter sized particles were rapidly excreted from the lungs.[41] For synthesis and in vitro testing of NCs, PLGA NPs ranging from 150−200 nm were formulated and used. Negatively stained transmission electron microscopy (TEM) images show the coating of NFs on the surface of the PLGA NPs in the TEM images (Figure 2b). Cryo-TEM further confirmed the structure, although with a lower contrast (Figure S2). This is important evidence showing the stability of NFs upon physical interactions with PLGA NPs.

The interaction between NFs and NPs was further confirmed by the increase in size and reduction in the surface charge of NCs (Figure 2a). Similar trends of reduction in the surface charge were observed in a recent study by Galindo et al., where targeted peptides were conjugated onto PLGA NPs for ocular delivery purposes.[41] We also confirmed the presence of peptide NFs on the PLGA NPs by using FITC-labeled NFs (Figure 2c). Our results show FITC-labeled NFs co-localized with Rhodamine B-labeled PLGA NPs (Figure 2c).

Furthermore, to confirm the formation of NCs in which NFs are physically attached on the NPs, NPs were freeze-dried, and Fourier transfer infrared (FT-IR) spectroscopy was performed to detect the presence of functional groups presented on the peptide NFs. A FT-IR spectrum of NCs showed a distinct peak of amide I groups at 1640 cm^{-1} along with (C−H) bending from the tryptophan rings seen at 750 cm^{-1}. These peaks are absent in PLGA NPs without NF coating (Figure 2e). Characteristic IR absorption of PLGA was observed for the −CH aliphatic bond stretching at 2850−2950 cm^{-1} and −C═O carbonyl stretching (Figure 2e). We used the microscale thermophoresis technique to investigate the interaction between NFs and PLGA NPs.[42] Here, thermophoretic kinetics of Rhodamine B-labeled NPs in the presence of different concentrations of NFs were followed. As sample concentrations of NFs used increased, the movement of Rhodamine B-labeled PLGA NPs was reduced in the presence of infrared laser pertaining to the binding of NFs onto PLGA NPs, whereas at lower concentrations of NFs or the NP only group, faster movement of NPs was shown with lower F_{norm} values (Figure 2d). Lower F_{norm} values were observed until a concentration of 7.81×10^{-6} M, and then, there is a jump showing higher F_{norm} from the interaction between NFs and NPs. A slight reduction of F_{norm} values was observed due to intrinsic tryptophan fluorescence from increased NF concentrations (Table S1). A similar behavior of intrinsic tryptophan fluorescence interference with F_{norm} values was previously observed by Chatterjee and Mandal.[43] Any change in the initial fluorescence and background buffer fluorescence was verified by initial capillary scans. No fluorescence from buffer or parity in the initial fluorescence from test samples was observed (Figure S3). The reduced movement of NPs in the presence of infrared laser is due to the bound NFs from electrostatic interactions with PLGA NPs.

2.2. In Vitro Evaluation of NC Uptake in Lung Epithelial Cells. Current lung disease treatment strategies involving systemic administration of drugs have low patient compliance and are associated with side effects. Hence, there is a need to develop effective drug delivery systems with the ability to overcome the various tissue/cell barriers for enhanced cell delivery efficacy.[44−46] CPPs have been proven effective for intracellular drug delivery; however, at higher concentrations, they suffer from severe toxicity due to their membrane perturbations.[47] Therefore, we set out to investigate the cytocompatibility of our new NCs compared with NFs and NPs alone in lung cells in vitro. This is a critical study for many other experiments as we compare our NCs with NPs (NPs) with respect to uptake and subsequently, drug delivery ability associated with improved uptake. Lung epithelial cells were chosen as a model due to their significance in maintaining a barrier to circulation, which is often disrupted by various virulence factors such as methicillin-resistant *Staphylococcus Aureus* (MRSA), Alpha-toxin (Hla), and Staphylococcal protein A (Spa) as well as viral pathogens such as SARS-CoV-2. NCs with a conjugation efficiency of ∼30% upon mixing of NFs and NPs (1:4 by mass or charge) were used as an optimum formulation for all the studies. Optimal formulation was found by validating the conjugation efficacy from various ratios of NFs/NPs and their uptake efficacy. Compared with plain NPs, the NCs did not show any significant change in cytocompatibility up to 1 mg/mL in primary lung AT1 epithelial cells compared to the untreated control, whereas NFs showed significant toxicity with

https://doi.org/10.1021/acsami.2c15204
ACS Appl. Mater. Interfaces XXXX, XXX, XXX−XXX

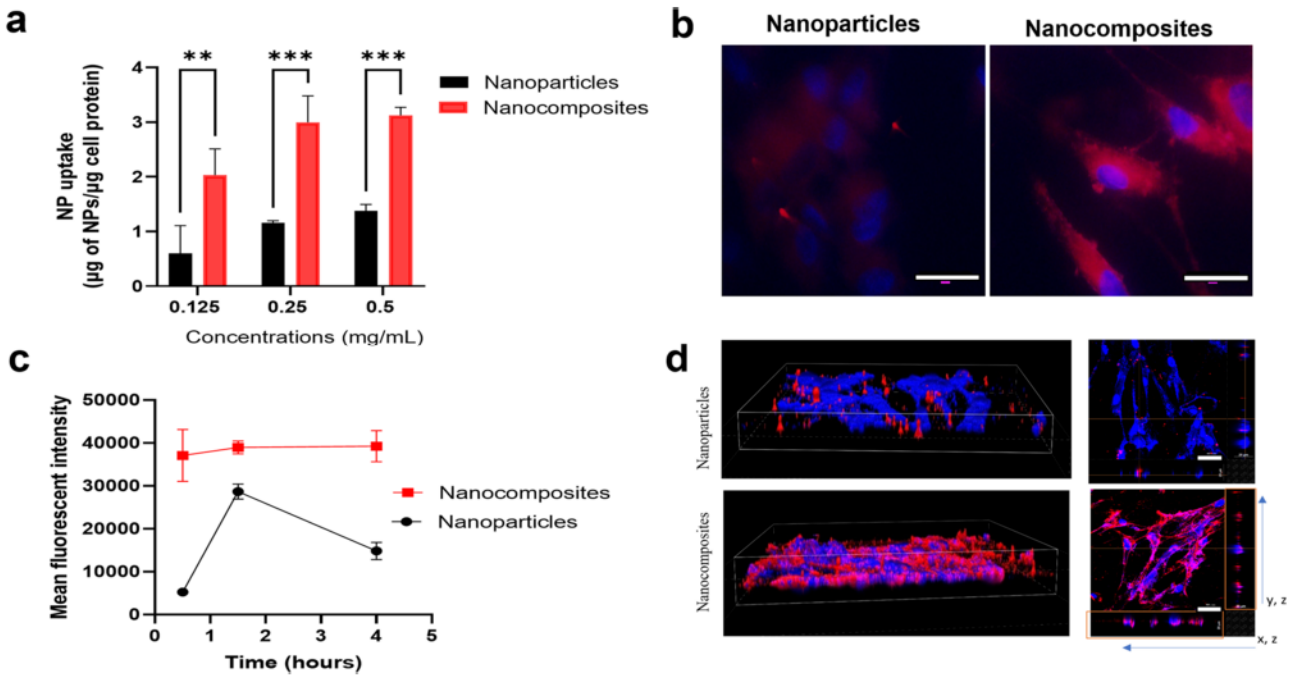

Figure 3. Cellular uptake of NCs. (a) NPs with NF coating (NCs—red bars) and without NFs (NPs—black bars) were given at various concentrations (0.125–0.5 mg) to overnight cultured primary lung Alveolar Type 1 epithelial cells and quantified by normalizing the Rhodamine B dye fluorescence from the cell lysate of each group with the respective cell protein content. (b) After 90 min, both groups of cells (nuclei, NCs/NPs) were washed three times with PBS and stained with DAPI to take images with a fluorescent microscope (scale 20 μm). (c) NPs and NCs were given to confluent Alveolar Type I cells seeded in a 48-well plate. At various time points of 30 min, 90 min, and 4 h, cells were washed and lysed to quantify fluorescent particles using a plate reader, and the cell protein from each well was used for normalization and plotting uptake kinetics. (d) 3D reconstruction of a confocal analysis of Alveolar epithelial cells exposed to NPs (top) and NCs (bottom) along with 3D reconstruction of *x*, *z* and *y*, *z* slices of the corresponding regions of image 2.5A showing the internalization of NPs (top) and NCs (bottom) with an increased amount seen in NCs. Scale bar *x*, *y*—50 μm, *x*, *z*—20 μm, and *y*, *z*—20 μm.

concentrations ranging from 0.25 to 1 mg/mL (Figure S3). NCs showed excellent cytocompatibility up to 1 mg/mL with RAW macrophages and human umbilical vein endothelial cells (HUVEC) (Figure S4). Based on the toxicity profile of NFs, NPs, and NCs, we presume that the NCs interact with cells in a different mode compared to free NFs, which typically involve membrane disruption and permeation as the initial step toward cell–material interactions.[48] Most likely, the improved cytocompatibility is largely due to the reduction of the overall charge upon physical complexation of the positively charged NFs and negatively charged NPs (Figure 2a). Based on this result, it suggests that combining positively charged membrane-permeating NFs with cytocompatible NPs can reduce the membrane disruptive activity of NFs and alleviate their toxicity toward cells, in particular lung epithelial cells used in the current study for pulmonary drug delivery. It is also noteworthy that even with the overall charge of NCs being negative, the cell uptake efficacy was dramatically enhanced, which will be discussed below.

The ability of NCs to improve cellular uptake was studied in primary lung epithelial cells, RAW macrophages, and HUVEC endothelial cells. These commonly found cell line types were used to assess the enhanced drug delivery abilities of NCs toward pulmonary drug delivery. Both AT1 and RAW macrophages showed a threefold and twofold increased uptake of NCs (labeled with Rhodamine B dye) compared to NPs (also labeled with Rhodamine B dye), respectively (Figures 3a and S6a). RAW macrophages, due to their intrinsic phagocytic activity, showed a higher uptake of NCs compared to lung epithelial cells (Figure S7a). NCs clearly had increased uptake in epithelial, macrophage and endothelial cells, which are the major cell types encountered when treating for pulmonary pathologies (Figures 3b and S7a-c). A dose-dependent study with various concentrations of NCs (30–500 μg) using epithelial cells showed that even at a ratio of 1:128, NFs and NPs still can improve the intracellular delivery of NCs indicating the NFs superior ability to interact with the cell membrane to internalize NPs and deliver associated payloads such as drugs or other biomolecules (Figure S5). These data show that cell membrane penetrating NFs, when coated onto NPs, can improve their delivery to cells and subsequently, the drugs cargo, enhancing intracellular drug delivery.

The kinetics of cell uptake was performed over 4 h to understand the time-dependent uptake in lung epithelial cells. This study helps to understand dosage time required, and design therapeutic dosages needed to be delivered to the cells. NCs immediately attached to the cells within 30 min and later were internalized by the cells over a 24 h period. Unlike NCs, NPs without NF coating showed a linear increase in uptake until 90 min, and later plateaued with reduction in NP internalization (Figure 3c). This reduction may be due to various phenomena such as exocytosis of NPs as extracellular vesicles or other mechanisms.[3]

NC uptake was further assessed using confocal laser scanning microscopy (CLSM) to validate the internalization. *Z*-stack 3D confocal cross-sections of AT1 cells (Figure 3d) showed that Rhodamine B-labeled NCs were localized next to the DAPI stained nucleus. The *x*, *z* and *y*, *z* slices (marked with red boxes in Figure 3d) demonstrated that the NCs were localized both intracellularly and extracellularly all over the

https://doi.org/10.1021/acsami.2c15204
ACS Appl. Mater. Interfaces XXXX, XXX, XXX–XXX

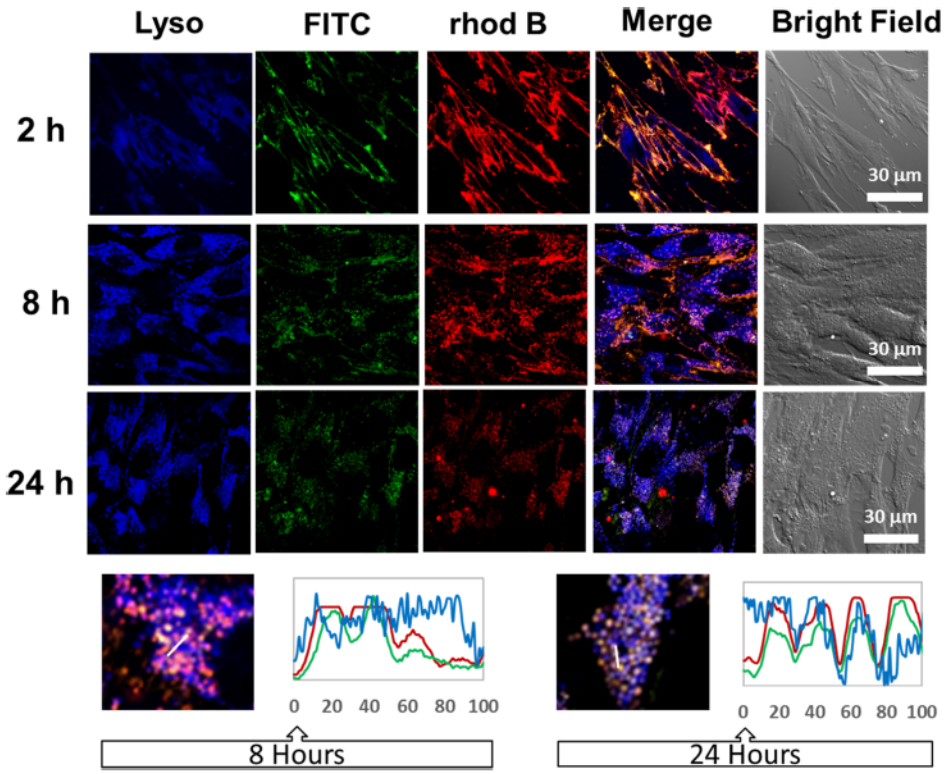

Figure 4. Endosomal escape of NCs. AT1 cells were seeded in confocal Petri dishes (1.1 cm^2) at confluency. The next day, NCs labeled with Rhodamine B and coated with FITC-labeled NFs were given to the cells and incubated for 2, 8, and 24 h. After each time point, cells were stained with Lysotracker blue and imaged using a confocal microscope. The merged image showed NCs attached to the cell membrane initially and later were internalized into the cell colocalization with lysosomes forming a purple color, which is evident from the intensity curves. After 24 h, more yellow color of NCs is seen, indicating the escape from lysosomes, also evident from the higher intensity of NCs (red and green color intensity).

treated cells, while in the NP group, the fluorescence level was much lower. The results indicated the coating of the NF dramatically increased both cell membrane bonding and cell uptake over a short period of time.

2.2.1. Lysosome Escape of NCs. Most of the drugs exhibit their functions in the cytoplasm or nucleus. The ability of a nanocarrier to achieve endosome/lysosome escape plays a vital role in determining their delivery efficiency. To investigate the escape of the NCs from lysosomes with various treatment times, CLSM images were analyzed to correlate fluorescence distribution and intensity between NCs, which were constructed with FITC-labeled NFs (green) and rhodamine-labeled NCs (red), and a lysosome tracker (blue). As shown in Figure 4, after 2 h of incubation, a yellow fluorescence was observed on the cell membrane due to the overlay of red fluorescence from the NP and green fluorescence from the NF. This result also suggests the physical stability of the NCs in the cellular microenvironment with the NF physically attached onto the NPs. With the increase of incubation time to 8 h, a pink fluorescence signal was seen in the cytoplasm, indicating co-localization of the lysosome and NCs. Upon 24 h of incubation, a yellow-to-white fluorescence signal was predominant which is indicative of NC escape from the lysosome, while the NFs and NPs were still physically complexed together within the NCs. An analysis of fluorescence intensity distribution shows the blue fluorescence is mostly merged with the green(NF) and red(NP) fluorescence's at 8 h, while at 24 h, the green and red fluorescence was shifted and dislocated with the blue fluorescence peak. This result is another evidence of time-dependent lysosome escape of NCs.

2.2.2. NC Uptake Mechanism in Lung Epithelial Cells. A study of the uptake mechanism in NCs can help understand the delivery efficiency and translation of results in other cell types.[4] Most NPs are internalized by cells using endocytic or phagocytic pathways, including clathrin, caveolin, micropinocytosis, and other energy-independent pathways. Previous studies have showed that self-assembled NFs undergo cell uptake by micropinocytosis in HeLa cells.[32] Given the new structure and composition of NCs, we screened the NCs for their uptake mechanisms using various endocytosis inhibitors. Lung epithelial cells after treatment with various endocytosis inhibitors and low temperature were treated with NCs. Similar to the free NF activity in HeLa cells, macropinocytosis inhibitors of cytochalasin-D showed a significant reduction in cellular uptake compared to that of untreated cells (Figure 5a). Comparable to our observations, actin filaments in epithelial cells, such as Madin–Darby canine kidney (MDCK) kidney cells, were shown to be critical in endocytic events where polymerization of actin filaments aids in absorption of material via macropinocytosis.[49] Cytochalasin-D inhibits the polymerization of these actin filaments in epithelial cells and significantly inhibits the NC uptake, which was also previously reported in A549 cells.[50] Our data show that NCs are up taken by macropinocytosis by the lung epithelial cells, which were previously shown to be capable of undergoing macropinocytosis.[51] To note, some of the macropinocytosis inhibitors did not show a significant difference to the untreated cells, which shows the altered effects of inhibitors in various cell lines.[4] Additional uptake inhibition studies were performed, where lung epithelial cells were incubated at 4

https://doi.org/10.1021/acsami.2c15204
ACS Appl. Mater. Interfaces XXXX, XXX, XXX−XXX

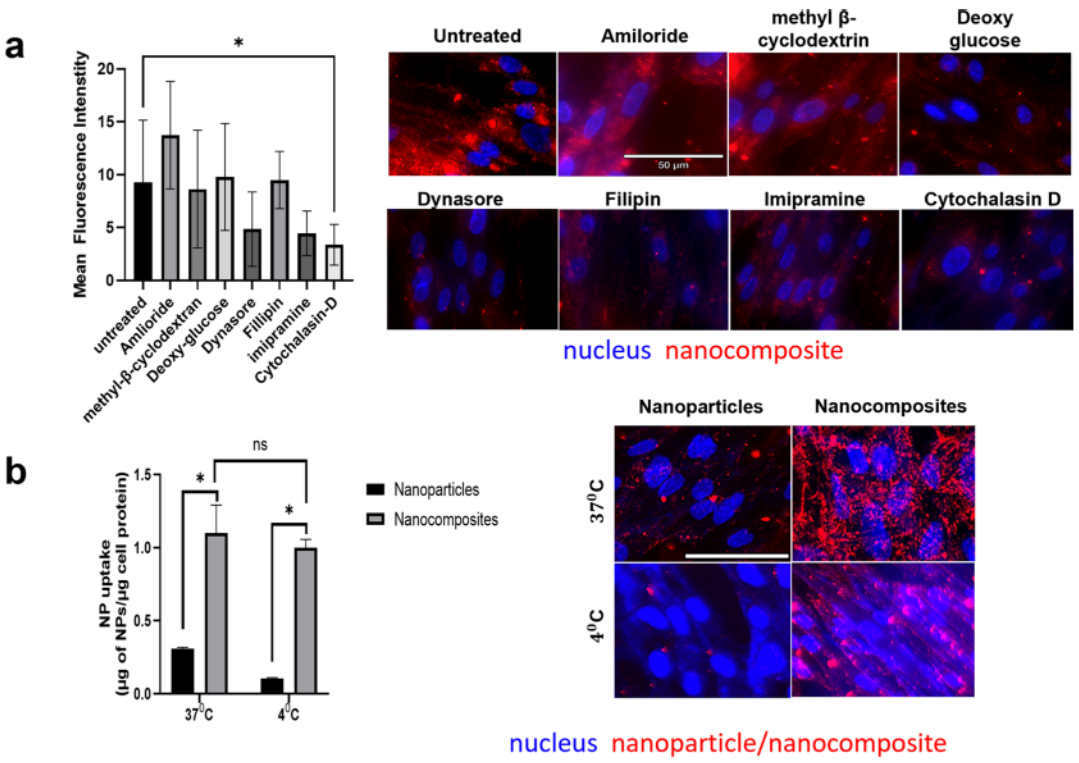

Figure 5. Cell uptake mechanism study. (a) Mean fluorescence intensity of uptaken NCs after treating cells with various endocytosis inhibitors for 2 h and allowing the NCs to uptake for 90 min. NucBlue stained nucleus and Rhodamine B-labeled NCs show a representative image of NC uptake in AT1 cells (scale 50 μm). Multiple comparisons done using Holm−Sidak's multiple comparison test. *$p < 0.05$, **$p < 0.01$ and multiple T test performed for freeze-dried NPs and NC uptake *$P < 0.0001$. (b) To assess the endocytosis and energy-dependency of cells for NC uptake, we performed cell uptake at 37 and 4 °C. For 4 °C, we pre-cooled the cells for 30 min and later quickly added NPs and NCs at 0.5 mg/mL and incubated for 90 min. Cells were washed and lysed, and then, fluorescence was recorded for uptake. Similarly, nuclei were stained with DAPI (Invitrogen) and imaged with a fluorescence microscope to visualize the cell uptake of NCs (scale bar−50 μm).

°C prior to the addition of NCs to assess the energy dependency on uptake. Interestingly, cellular uptake of NCs was significantly higher than NPs showing a mixed energy-independent cell uptake mechanism along with macro-pinocytosis in physiological conditions (Figure 5b). Taken together with cell uptake studies, the results show that NF coating allows the NCs to immediately attach to the cell membrane and slowly aids NPs to enter cells via macro-pinocytosis or passive cell membrane passage in a non-energy dependent fashion.

2.2.3. Mucus Permeation of NCs. Penetration of the mucus layer is highly desired to reach the injured epithelium in lungs due to the diseased state including infections and fibrotic conditions, among others. Especially in the case of lung infections, mucus hypersecretion is observed due to an increase in inflammatory signaling.[52] Hence, it is vital to understand the mucus permeation of NCs. Adhesion of NPs to the mucus fiber is a challenge, and control over the size of the NP can improve the permeation. Recent reports suggest that NPs <500 nm with a mucus inert coating can navigate through the mucus layer.[53] Here, we assessed the mucus permeation of NPs with and without the NF coating using a simulated mucus layer (Figure 6). NCs labeled with Rhodamine B were layered on top of simulated mucus, and their permeation through mucus and a 0.4 μm pore size transwell into the lower chamber was recorded to assess permeation kinetics. NCs traversed at a significantly higher rate compared to NPs until 8 h, and later, the permeation rate was similar to NP permeation with and without the NF coating using a simulated kinetics (Figure 6). Overall, more NCs permeated through the mucus than the NP alone, showing that NFs may interfere with NP binding to mucin proteins.

2.2.4. Translative Potential of NCs. NP-based drug delivery systems are being developed at an ever-increasing rate, but very few have reached the clinical trial stage.[54] This is due to the challenges associated with translation such as large-scale manufacturing, stability, delivery, and safety, among others. Here, we assessed the stability in storage and nebulization for their potential in pulmonary drug delivery. Freeze-drying of NCs still showed significantly higher uptake in lung epithelial cells compared to NPs (Figure 7d), demonstrating the storage ability of NCs in the powder form. NCs also showed higher uptake compared to a conventional cell membrane penetrating HIV TAT peptide-coated NPs (Figure 7e). This indicates the superior ability of the NFs to improve NP affinity toward the cell membrane. NCs in powder possess higher stability after modifications compared to NPs, suggesting stability of the NF binding of NPs after undergoing freeze-drying and storage at −20 °C. For nanocarriers such as the NCs developed here, inhalation has recently gained attention as an ideal mode of pulmonary drug delivery.[55,56] To assess the abilities of NFs to improve the NP uptake in cells when nebulized, NCs and NPs were delivered to lung AT1 cells in vitro via a lab module nebulizer generating droplets of size 2.5−4 μm (Figure 7a).[57] NCs delivered via nebulization showed improved uptake with deposition efficiency over 23% delivered compared to 3% of NPs (Figure 7b,c). Low retention of NPs compared to NCs can be explained by the higher negative charge, which may

https://doi.org/10.1021/acsami.2c15204
ACS Appl. Mater. Interfaces XXXX, XXX, XXX−XXX

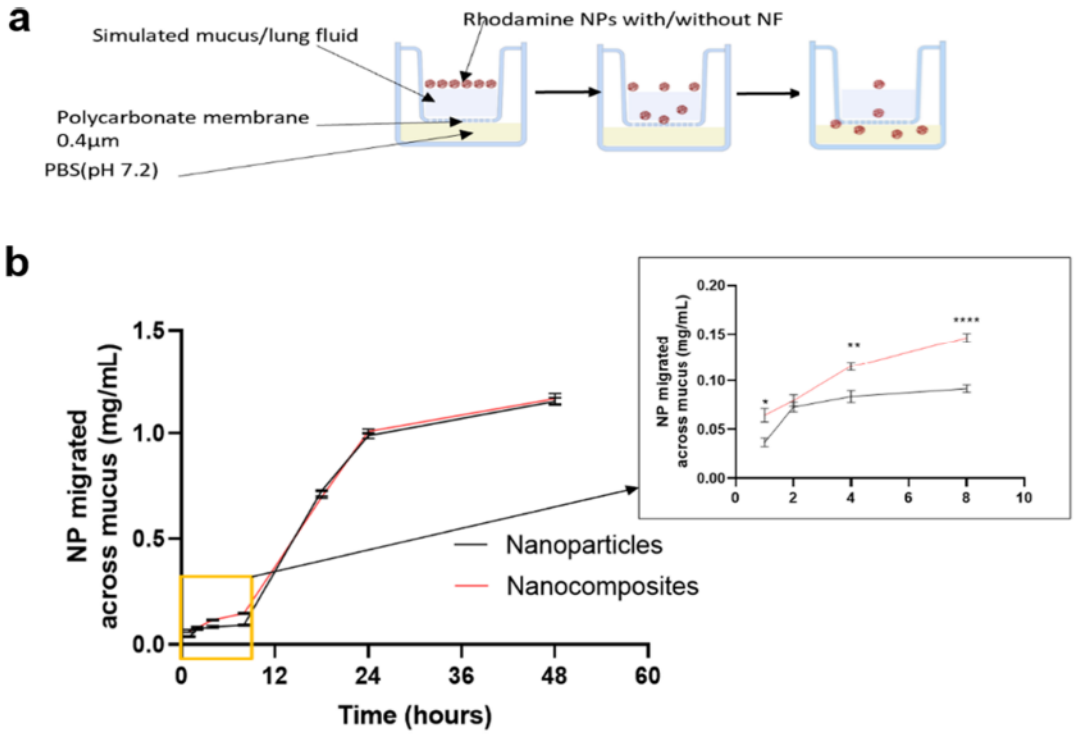

Figure 6. Mucus permeation study. (a) Schematic of mucus penetration setup. (b) 50 μL of NPs or NCs loaded with Rhodamine B dye at 10 mg/mL were laid on top of simulated mucus in a transwell plate with 0.4 μm pore size, with PBS in the lower layer. At various time points (0–48 h), lower PBS solution was collected and measured using a plate reader. NCs had a greater penetration initially until 8 h and later followed similar penetration kinetics as NPs. (*P < 0.05, **P < 0.01, ****p < 0.0001).

pose an interaction issue with the material used for delivering particles to the well plate and loss of samples during nebulization. The amount of NCs that reach the media after loss during nebulization have higher affinity toward cell membrane and are up taken at a higher rate. Other studies of in vitro nebulization showed fluorescein deposition efficiency of <10%, which is comparable to the ones observed in NPs.[57] Nebulization studies in vitro showed that NCs delivered via inhalation have the potential to enhance pulmonary drug delivery compared to PLGA-based NPs.

3. CONCLUSIONS

Our findings demonstrate that using NFs made from de novo self-assembled peptides and coating them on polymer NPs such as PLGA NPs can improve NP uptake in lung epithelial cells in vitro. These NF coatings effectively improve NP uptake in macrophages along with endothelial cells. Both cell lines respond to bacterial pathogens and have high activity in lung diseases such as bacterial and viral infections. In addition, the NCs can be delivered across a simulated mucus layer, showing the ability to permeate the mucus layer effectively. With the evident potential for translation seen in freeze-drying and nebulization studies, these NCs can be extended to develop the next generation of pulmonary drug therapeutics involving advanced gene and drug delivery to treat a variety of lung diseases. Further modification of NFs can include targeted approaches with functional peptides and other NP conjugation strategies.

4. EXPERIMENTAL SECTION

4.1. Materials. All chemicals, if not specified, were purchased from Sigma-Aldrich (St. Louis, MO). PLGA (copolymer ratio 50:50, molecular weight 15–25 kDa) was purchased from Akina Inc. (West Lafayette, IN); Rhodamine B dye was purchased from Sigma-Aldrich (St. Louis, MO); and the NFs were synthesized in-house as previously described.[32] Primary human alveolar type 1 cells were obtained from Applied Biological Materials (Richmond, BC, Canada). Iscove's modified Dulbecco's medium (IMDM), fetal bovine serum, penicillin–streptomycin, and trypsin-ethylenediaminetetraacetic acid (EDTA) were procured from Fischer Scientific (Waltham, MA). Amiloride, filipin III, and methyl-β-cyclodextrin were purchased from Sigma-Aldrich (St. Louis, MO).

4.2. Synthesis of NCs. A double emulsion method as described by Messerschmidt et al. was employed for the synthesis of PLGA NPs.[58] First, 100 mg of PLGA polymer (Polyscitech, West Lafayette, USA) was dissolved in dichloromethane at 100 mg/mL. 1% (w/w) Rhodamine B (Rho B) (Sigma-Aldrich, St. Louis, USA) was prepared as a water phase, which was later added dropwise into the oil-phase of the PLGA solution. This primary solution was sonicated to form the primary emulsion. The primary emulsion was then emulsified into 5% (w/v) poly(vinyl) alcohol (PVA, 13KDa) solution via sonication at 35 W for 4 min (30 s off every 1 min). Rho B-loaded PLGA NPs were collected by centrifugation at 15,000 rpm for 15 min and then lyophilized until completely dry.

NFs were synthesized as previously described.[32] Briefly, a standard Fmoc-solid phase peptide synthesis method was employed, and the synthesis was carried out on a Prelude peptide synthesizer. The peptide was terminated with either an acetyl group or FITC. The acetylated peptide is denoted as non-labeled peptide and FITC terminated peptide is denoted as labeled peptide for the following procedures. All peptides were purified by high-performance liquid chromatography (HPLC) followed by lyophilization. The molecular weight of each peptide was confirmed by MALDI-TOF mass spectrometry using α-cyano-4-hydroxycinnamic acid as the matrix. Acetylated $K_{10}(QW)_6E_3$: expected $[M + H]^+$: 3612.9, observed $[M + H]^+$: 3611.2; FITC terminated $K_{10}(QW)_6E_3$: expected $[M + H]^+$: 3928.9, observed $[M + H]^+$: 3629.23.

Non-labeled peptides were dissolved in tris(hydroxymethyl)-aminomethane) (Tris) buffer (pH 7.4, 20 mM) buffer at 20 mM

https://doi.org/10.1021/acsami.2c15204
ACS Appl. Mater. Interfaces XXXX, XXX, XXX–XXX

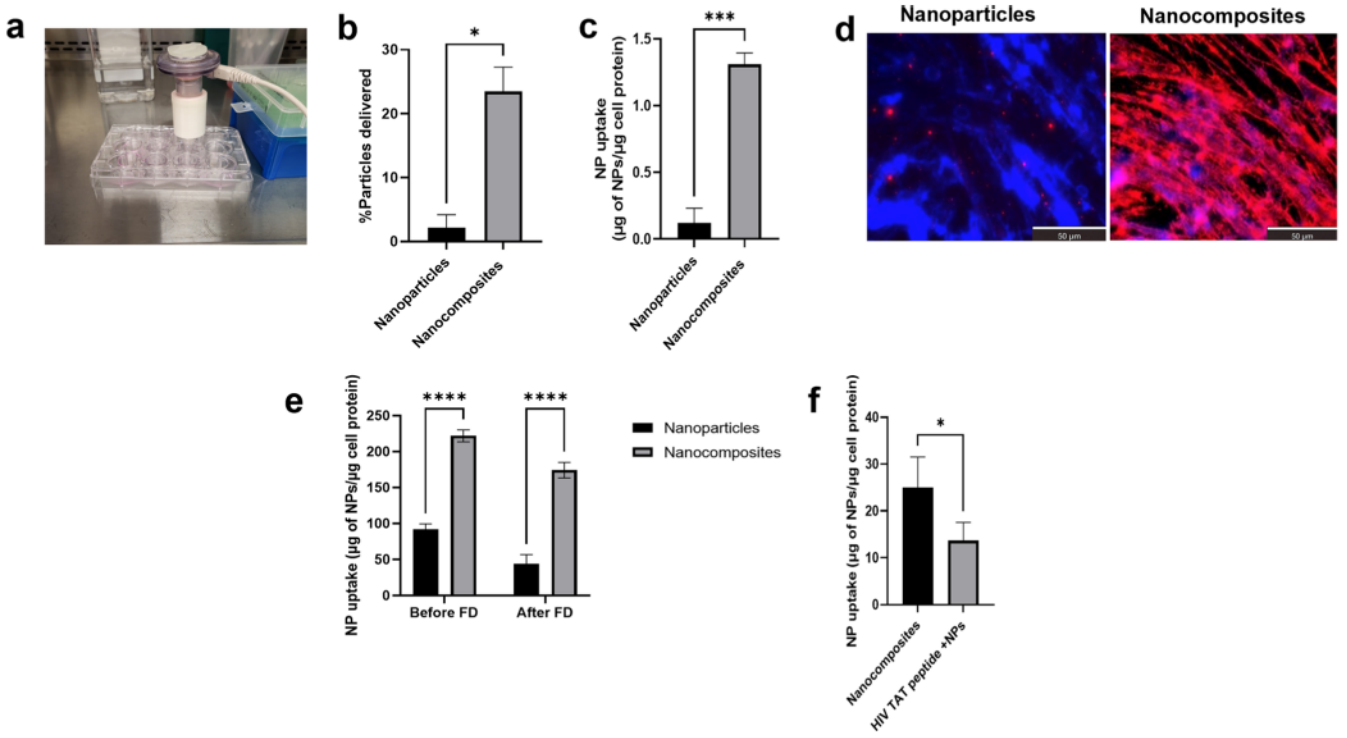

Figure 7. Translative potential of NCs. AT1 lung epithelial cells were seeded at confluency in a 12-well plate and grown overnight. 1 mg/mL of NCs were nebulized using an Aeroneb lab module nebulizer to generate droplets of size 2.5−5 μm. After 90 min, cells were washed three times with PBS and stained with DAPI to visualize the uptake. Later, cells were lysed to analyze NP uptake by a fluorescent reading using a photofluorescent plate reader, and the measurements normalized against cell protein. (a) Image showing nebulizer and 3D printed extension attached to deliver NPs and NCs to cells in a 12-well plate. (b) % uptake after delivery of NPs and NCs via nebulization (paired *t*-test $*p < 0.05$). (c) NP/NC uptake after nebulization in AT1 cells after normalization with cell protein in each group. (d) Fluorescent images after nebulization showing cell nuclei stained with DAPI and NPs loaded with Rhodamine B (scale 50 μm). (e) Before and after freeze-drying effects on cellular uptake of both NPs and NCs show NCs retain ability of higher uptake even after freeze-drying (two-way ANOVA with Sidak's multiple comparison was done with $****p < 0.0001$). (f). Comparison on effects of NF and TAT peptide coating. NF coating shows a significantly higher uptake of NPs in AT1 cells compared to HIV TAT cell membrane penetrating peptide available commercially (paired *t*-test $*p < 0.05$).

concentration and incubated for a period of 12 h to self-assemble into NFs. NFs containing labeled peptides were prepared by mixing a non-labeled peptide with a FITC-labeled peptide with a molar ratio of 90:10 in a mixed solvent of water and acetonitrile (1:1 by volume). The mixture was lyophilized and rehydrated in Tris buffer (pH 7.4, 20 mM) to reach a final concentration of 1 mM and left at 4 °C for 12 h.

After lyophilization of NPs, 2 mg of Rho B-NPs was dissolved in Tris buffer and 0.5 mg of NF in suspension was added to the NP suspension. The mixture was left to react electrostatically by rotating the solution for an hour at room temperature. Later, the sample was centrifuged at 15,000 rpm for 7 min to remove free NFs and collect the NCs which contained NF-coated Rho B-loaded NPs.

Plain PLGA NPs used for FT-IR studies were synthesized by a single emulsion method where the PLGA polymer was dissolved in chloroform followed by dropwise addition into 5% (w/v) PVA. The mixture was emulsified via sonication at 35 watts for 4 min (30 s off every 1 min). Later, the PLGA NPs were collected via centrifugation and lyophilized until dry.

4.3. Characterization of NCs. *4.3.1. DLS Measurements.* ZETAPALS90 dynamic light scattering (DLS) detector (Brookhaven Instrument, Holtsville, NY) was used to determine size, charge, and polydispersity of the NCs. For DLS measurements, 50 μL of 1 mg/mL NC suspension was mixed with 3 mL of DI water in a transparent cuvette and placed in the instrument to measure size, while a DLS probe was used to measure the zeta potential of the NCs.

4.3.2. Fluorescent Microscopy. Fluorescein terminated peptides were synthesized as previously described by Yang and Dong.[32] 5(6)-Carboxyl fluorescein (FITC)-tagged peptides were mixed with Rho B PLGA NPs. Green color tagged NFs were incubated with NPs loaded with Rhodamine B (red color). The NCs formed were washed three times to remove any unbound NFs. Another set of NPs were similarly washed and imaged without any NF. A fluorescent microscope (ECHO, San Diego, CA) with FITC (for NF) and Texas Red channels (For Rho B NPs) at 100× magnification was used to image the NF coating on the NPs.

4.3.3. Cryo-Electron Microscopy. Cryo-EM grids were prepared using a Vitrobot Mark IV plunge-freezer (Thermo Fisher Scientific). Three microliters of the sample were applied to Lacey carbon grids (300-mesh; Ted Pella, Inc.) that were glow discharged at 30 mA for 80 s. Grids were blotted at 95% relative humidity for 4 s prior to plunge freezing. The sample grids were imaged on a Talos Arctica 200 kV transmission electron microscope (Thermo Fisher Scientific) equipped with a Gatan K3 camera (Gatan, Inc.). The nominal magnification is at 45,000×, which corresponds to a pixel size of 0.88 Å.

4.3.4. FTIR of NCs. Freeze-dried material including PLGA polymers, plain PLGA NPs, NCs, and NFs were analyzed using Fourier-transform infrared (FTIR) spectroscopy. Briefly, FTIR spectra of the varied materials were recorded in the transmission mode using FT-IR Nicolet-6700 in the range of 400−4000 cm^{-1}.

4.3.5. Binding Kinetics of NFs to NPs. Thermophoresis technique was used to detect the binding of NFs (ligand) to the NPs. F_{norm} represents the change in thermophoresis, which is expressed as a change in thermophoresis when non-fluorescent ligand titration is introduced to fluorescent NPs.[42] Here, NF titrations were made starting from 2 mg/mL of NFs up to 10 dilutions with NP concentration kept constant at 2 mg/mL for all the titrations. A small capillary tube was used to load ~4 μL of the various NF−NP combinations and placed in the loading tray of a Thermophoresis instrument Monolith NT.115 (NanoTemper Technologies, Inc., San

https://doi.org/10.1021/acsami.2c15204
ACS Appl. Mater. Interfaces XXXX, XXX, XXX−XXX

Francisco, CA). To determine the position of the capillaries, a fluorescence scan was performed. Subsequently, thermophoresis measurements were performed to determine the binding kinetics of NFs to NPs. F_{norm} was calculated by the machine along with various other parameters including binding constant.

4.4. Cytocompatibility of NCs. Here, primary lung epithelial cells, RAW macrophages, and HUVEC endothelial cells were used to assess toxicity from NCs. NCs were prepared as described in Section 2.2.2, where 20,000 cells/well of primary alveolar type I epithelial cells (AT1) were seeded in 48-well plates. After the overnight culture, various groups of particles including plain/blank PLGA NPs, NFs only, and NCs (NF coated PLGA NPs) were given to the cells in triplicates at various concentrations ranging from 0.0625 to 1 mg/mL. The NF concentration was chosen equivalent to the peptide amount conjugated onto the NPs. After 72 h, cells were washed three times with PBS, and MTS reagent was given to the cells to assess the cell viability following the company's instructions.

4.5. Cellular Uptake of NCs. The cellular uptake study was performed as described previously by Iyer et al.[59] NCs made from Rhodamine B PLGA NPs, and NFs were used as fluorescently labeled NCs for cell uptake studies. Cell uptake of NCs was determined by measuring internalized fluorescent NCs. Various cell lines representative of the lower respiratory tract, including AT1 and RAW macrophages, were used to assess the NC cell internalization ability compared with plain/blank NPs. AT1 cells (15,000 cells/well) and RAW cells (20,000 cells/well) were seeded onto a 48-well plate and were grown overnight at 37 °C. After overnight attachment, various NPs and NCs with different concentrations (0, 50, 100, and 250 μg/mL) in media were given to the cells for 90 min. After 90 min, AT1/RAW cells were washed three times with PBS and lysed using 2% Triton X-100. Fluorescence intensities of internalized NPs or NCs were measured at a wavelength of λ_{ex} 546 nm and λ_{em} 585 nm (for the Rhodamine B fluorescence loaded into the NPs/NCs). Cell lysate was also used to determine the protein content using bicinchoninic acid (BCA) assays per the manufacturer's instructions (Pierce BCA Protein Assay, Thermo Scientific).

For visualizing the cellular uptake before the cell lysis, the cells were stained for the nucleus with NucBlue (Thermoscientific) for 20 min. After staining, cells were imaged using a fluorescent microscope (ECHO, San Francisco, CA) in the DAPI channel for the nucleus and the Texas Red channel for NPs or NCs.

Time-dependent uptake of NCs in comparison with NPs was performed in lung epithelial cells. Briefly, AT1 cells were seeded at confluency and allowed to attach overnight. The next day, cells were treated with 0.5 mg/mL NCs or NPs for uptake. At time points of 30 min, 90 min, and 4 h, cells were washed three times with PBS and lysed with 2% Triton X-100. Cell lysate was read for fluorescent particles using a plate reader. Later, the total cell protein content was measured using a BCA assay.

AT1 cells were seeded at confluency onto a glass slide to perform confocal studies for NC uptake. After overnight attachment, NCs or NPs at a concentration of 0.5 mg/mL were incubated with the cells for uptake. Cells were washed three times with PBS after 4 h of uptake, and the cell nucleus was stained with NucBlue. Cells on the glass slide were mounted with a cover slip to visualize the internalization of NCs using a Nikon A1R confocal microscope.

AT1 cells were seeded on a confocal dish to perform the lysosome escape study. After overnight attachment, NCs were incubated with the cells at a concentration of 0.5 mg/mL. For all incubation times, the medium was changed at 2 h to keep consistent cell uptake quality. After 2, 8, and 24 h incubation, cells were washed with PBS three times. Lysosomes were stained with LysoTracker Blue DND-22 (Invitrogen) for 30 min and followed by three times PBS wash. The internalization of NCs was visualized using a Nikon A1R confocal microscope.

4.6. NC Cellular Uptake Mechanism Study. To determine the NC/NP uptake mechanism used by cells, endocytosis-inhibition study was performed. Alveolar Type I cells were seeded at confluency in 48-well plates and attached overnight at 37 °C in an incubator with 5% CO_2. Rhodamine B-loaded NCs were prepared using a similar procedure done for other studies. After 24 h of seeding, the AT1 cell culture medium was replaced by fresh 1% serum media containing 5 μM amiloride, 5 μM methyl-β-cyclodextran, 5 μg/mL filipin III, 5 μM cytochalasin-D, 5 μM imipramine, 80 μM dynasore, or 5 mM deoxyglucose (Sigma-Aldrich & Cayman Chemical). After 2 h, fresh complete media with Rhodamine B-labeled NCs was added at a concentration of 0.5 mg/mL. After 12 h, cells were washed with PBS and nuclei stained with NucBlue (Thermo Fisher). Images were acquired using a fluorescent microscope and processed for NP uptake random areas from 10 images of each inhibitor group with ImageJ software.

In a similar fashion, to check if the NC undergoes an energy-dependent uptake, the temperature block was studied in AT1 cells by preincubating cells at 4 °C for 30 min, followed by treatment with fluorescent NCs for 90 min at 4 °C. Later, fluorescent images were acquired, and the cell lysate was analyzed for quantitative NC uptake.

4.7. Mucus Permeation Study. A mucus permeation study was performed to study the effects of the NF coating on the permeation of the NPs to mimic the in vivo environment. NCs/NPs loaded with Rhodamine B dye were used for the study. A 12-well transwell plate with a pore size of 0.4 μm was used for the study. Mucus was simulated based on previous literature.[60] Briefly, porcine mucin protein was mixed with salts, DNA and DPPC to form simulated mucus. 100 μL of simulated mucus was placed on the transwell membrane and 500 μL of PBS was placed in the lower chamber. 25 μL of 10 mg/mL NCs/NPs was placed on top of the simulated mucus to allow for permeation from the transwell to the lower chamber. PBS from the lower chamber was collected at various time points to measure the fluorescent NCs/NPs permeated through the mucus. Fresh PBS was replaced at different time points.

4.8. In Vitro Nebulization. To assess the cell uptake ability of aerosolized NCs, we used a lab module nebulizer (Aeroneb, Kent scientific, Torrington, CT) to deliver NCs and NPs. AT1 lung epithelial cells were seeded at 0.4 million cells/well in a 12-well plate and grown overnight. 1 mg/mL of both NCs and NPs in PBS were aerosolized using a lab module nebulizer from Aeroneb. Aeroneb generated 2.5−4 μm droplets of particulate suspension. After nebulization of droplets, cells were incubated at 37 °C for 90 min. After incubation, cells were washed with PBS and stained for the nucleus with NucBlue (Thermo Fisher). Fluorescent images were taken of the cells for uptake of NCs and NPs using a fluorescent microscope (ECHO, San Francisco, CA) under DAPI (nucleus) and Texas Red (NCs/NPs) channels. Later, the cells were lysed using 2% Triton X-100, and the cell lysate was read using a spectrophotometer at wavelengths of λ_{ex} 546 nm and λ_{em} 585 nm. The cell protein amount measured by protein assay was used to normalize the fluorescent readings from cells. Percentage of total delivered (100% = NP/NC delivered to cells) and weight number of NCs/NPs delivered to the cells were calculated based on the cell protein normalized fluorescence readings.

4.9. Effects of NC Freeze-Drying. A cell uptake study was performed to assess the ability of NCs to retain an enhanced uptake ability after freeze drying. NPs along with NCs loaded with Rhodamine B dye were freeze-dried until dry. Later, NPs and NCs from before and after freeze-drying were prepared using TRIS buffer and later washed and mixed with complete media. AT1 cells in 48-well plates grown to confluency were given various groups of NCs and NPs from before and after freeze-drying samples at a concentration of 0.5 mg/mL. A cell uptake study was performed similar to the previous procedure (see Section 4.5).

4.10. NF-Coated NPs versus HIV TAT Peptide-Coated NPs. HIV TAT peptide is a common CPP. This study was aimed to compare NF coating and HIV TAT peptide coating for enhanced cell uptake ability. HIV TAT peptide (Sigma-Aldrich, St. Louis, USA) coating of PLGA NPs was done similarly to the NF coating (see Section 4.2). Briefly, 0.5 mg of either HIV TAT peptide or NF was mixed with 2 mg of NPs by rotation at room temperature for an hour. Later, the NCs with the HIV TAT/NF coating were collected and mixed with complete cell culture media at 0.5 mg/mL. AT1 cells grown overnight at confluency were given the NC groups and allowed

https://doi.org/10.1021/acsami.2c15204
ACS Appl. Mater. Interfaces XXXX, XXX, XXX−XXX

to be uptaken for 90 min. A cell uptake study was performed similar to the previous procedure (see Section 4.5).

4.11. Statistical Analysis. GraphPad Prism 8 (GraphPad Software Inc., San Diego, USA) was used to perform all statistical analysis. One-way ANOVA with Sidak's multiple comparison, Dunnett multiple comparisons, and Tukey's multiple comparison tests were done for different data analyses as appropriate for the data sample. Triplicate samples were used for all the studies if not specified.

■ ASSOCIATED CONTENT

Supporting Information

The Supporting Information is available free of charge at https://pubs.acs.org/doi/10.1021/acsami.2c15204.

MALDI spectra of peptides, cryo-EM image of NCs, capillary scans of microscale thermophoresis, cytocompatibility of NCs in AT1 epithelial and HUVEC cells, dose-dependent uptake of NCs in lung epithelial cells, and NC uptake in RAW macrophages and HUVEC endothelial cells (PDF)

■ AUTHOR INFORMATION

Corresponding Authors

He Dong − *Department of Chemistry and Biochemistry, University of Texas at Arlington, Arlington, Texas 76019, United States;* orcid.org/0000-0002-8494-0475; Email: he.dong@uta.edu

Kytai T. Nguyen − *Department of Bioengineering, University of Texas at Arlington, Arlington, Texas 76010, United States;* Email: knguyen@uta.edu

Authors

Uday Chintapula − *Department of Bioengineering, University of Texas at Arlington, Arlington, Texas 76010, United States;* orcid.org/0000-0002-6028-4485

Su Yang − *Department of Chemistry and Biochemistry, University of Texas at Arlington, Arlington, Texas 76019, United States*

Trinh Nguyen − *Department of Bioengineering, University of Texas at Arlington, Arlington, Texas 76010, United States*

Yang Li − *Department of Biophysics, University of Texas at Southwestern Medical Center, Dallas, Texas 75390, United States*

Justyn Jaworski − *Department of Bioengineering, University of Texas at Arlington, Arlington, Texas 76010, United States;* orcid.org/0000-0001-9214-3671

Complete contact information is available at: https://pubs.acs.org/10.1021/acsami.2c15204

Author Contributions

‖U.C. and S.Y. have contributed equally to this project. All authors have given approval to the final version of the manuscript.

Notes

The authors declare no competing financial interest.

Data will be provided by the author upon request with acceptable reason.

■ ACKNOWLEDGMENTS

This work was partly supported by CPRIT RP210206 (K.T.N.) and NSF DMR1824614 (H.D.). We thank the Structural Biology Laboratory at UT Southwestern Medical Center which is partially supported by grant RP170644 from the Cancer Prevention & Research Institute of Texas (CPRIT) for cryo-EM studies. Biorender.com was used for graphical abstract and schematics.

■ REFERENCES

(1) Mitchell, M. J.; Billingsley, M. M.; Haley, R. M.; Wechsler, M. E.; Peppas, N. A.; Langer, R. Engineering Precision Nanoparticles for Drug Delivery. *Nat. Rev. Drug Discovery* **2021**, *20*, 101−124.

(2) Gelperina, S.; Kisich, K.; Iseman, M. D.; Heifets, L. The Potential Advantages of Nanoparticle Drug Delivery Systems in Chemotherapy of Tuberculosis. *Am. J. Respir. Crit. Care Med.* **2005**, *172*, 1487−1490.

(3) Oh, N.; Park, J.-H. Endocytosis and Exocytosis of Nanoparticles in Mammalian Cells. *Int. J. Nanomed.* **2014**, *9*, 51−63.

(4) Rennick, J. J.; Johnston, A. P. R.; Parton, R. G. Key Principles and Methods for Studying the Endocytosis of Biological and Nanoparticle Therapeutics. *Nat. Nanotechnol.* **2021**, *16*, 266−276.

(5) Abo-zeid, Y.; Williams, G. R.; Touabi, L.; McLean, G. R. An Investigation of Rhinovirus Infection on Cellular Uptake of Poly (glycerol-adipate) Nanoparticles. *Int. J. Pharm.* **2020**, *589*, 119826.

(6) Calvo, A.; Moreno, E.; Clemente, U.; Pérez, E.; Larrea, E.; Sanmartín, C.; Irache, J. M.; Espuelas, S. Changes in the Nanoparticle Uptake and Distribution Caused by an Intramacrophagic Parasitic Infection. *Nanoscale* **2021**, *13*, 17486−17503.

(7) Kirtane, A. R.; Verma, M.; Karandikar, P.; Furin, J.; Langer, R.; Traverso, G. Nanotechnology Approaches for Global Infectious Diseases. *Nat. Nanotechnol.* **2021**, *16*, 369−384.

(8) Vila-Gómez, P.; Noble, J. E.; Ryadnov, M. G. Peptide Nanoparticles for Gene Packaging and Intracellular Delivery. *Methods Mol. Biol.* **2021**, *2208*, 33−48.

(9) Jeong, W.-j.; Bu, J.; Kubiatowicz, L. J.; Chen, S. S.; Kim, Y.; Hong, S. Peptide−Nanoparticle Conjugates: A Next Generation of Diagnostic and Therapeutic Platforms. *Nano Convergence* **2018**, *5*, 38.

(10) Gessner, I.; Neundorf, I. Nanoparticles Modified with Cell-Penetrating Peptides: Conjugation Mechanisms, Physicochemical Properties, and Application in Cancer Diagnosis and Therapy. *Int. J. Mol. Sci.* **2020**, *21*, 2536.

(11) dos Santos Rodrigues, B.; Lakkadwala, S.; Kanekiyo, T.; Singh, J. Development and Screening of Brain-Targeted Lipid-Based Nanoparticles with Enhanced Cell Penetration and Gene Delivery Properties. *Int. J. Nanomed.* **2019**, *14*, 6497−6517.

(12) Kostiv, U.; Kotelnikov, I.; Proks, V.; Šlouf, M.; Kučka, J.; Engstová, H.; Ježek, P.; Horák, D. RGDS- and TAT-Conjugated Upconversion of NaYF4:Yb(3+)/Er(3+)&SiO2 Nanoparticles: In Vitro Human Epithelioid Cervix Carcinoma Cellular Uptake, Imaging, and Targeting. *ACS Appl. Mater. Interfaces* **2016**, *8*, 20422−20431.

(13) Kapur, A.; Medina, S. H.; Wang, W.; Palui, G.; Schneider, J. P.; Mattoussi, H. Intracellular Delivery of Gold Nanocolloids Promoted by a Chemically Conjugated Anticancer Peptide. *ACS Omega* **2018**, *3*, 12754−12762.

(14) Boussoufi, F.; Navarro Gallón, R.; Chang, T. J.; Webster, T. Synthesis and Study of Cell-penetrating Peptide-Modified Gold Nanoparticles. *Int. J. Nanomed.* **2018**, *13*, 6199−6205.

(15) Li, Y.; Hao, L.; Liu, F.; Yin, L.; Yan, S.; Zhao, H.; Ding, X.; Guo, Y.; Cao, Y.; Li, P.; Wang, Z.; Ran, H.; Sun, Y. Cell Penetrating Peptide-Modified Nanoparticles for Tumor Targeted Imaging and Synergistic Effect of Sonodynamic/HIFU Therapy. *Int. J. Nanomed.* **2019**, *14*, 5875−5894.

(16) Huang, H.-L.; Lin, W. J. Dual Peptide-Modified Nanoparticles Improve Combination Chemotherapy of Etoposide and siPIK3CA Against Drug-Resistant Small Cell Lung Carcinoma. *Pharmaceutics* **2020**, *12*, 254.

(17) Cui, H.; Webber, M. J.; Stupp, S. I. Self-Assembly of Peptide Amphiphiles: From Molecules to Nanostructures to Biomaterials. *Pept. Sci.* **2010**, *94*, 1−18.

(18) Hauser, C. A.; Zhang, S. Designer Self-Assembling Peptide Nanofiber Biological Materials. *Chem. Soc. Rev.* **2010**, *39*, 2780−2790.

(19) Rudra, J. S.; Tian, Y. F.; Jung, J. P.; Collier, J. H. A Self-Assembling Peptide Acting as an Immune Adjuvant. *Proc. Natl. Acad. Sci. U.S.A.* **2010**, *107*, 622−627.
(20) Yan, C.; Pochan, D. J. Rheological Properties of Peptide-Based Hydrogels for Biomedical and Other Applications. *Chem. Soc. Rev.* **2010**, *39*, 3528−3540.
(21) Branco, M. C.; Sigano, D. M.; Schneider, J. P. Materials from Peptide Assembly: Towards the Treatment of Cancer and Transmittable Disease. *Curr. Opin. Chem. Biol.* **2011**, *15*, 427−434.
(22) Hudalla, G. A.; Sun, T.; Gasiorowski, J. Z.; Han, H.; Tian, Y. F.; Chong, A. S.; Collier, J. H. Gradated Assembly of Multiple Proteins into Supramolecular Nanomaterials. *Nat. Mater.* **2014**, *13*, 829−836.
(23) Kumar, V. A.; Taylor, N. L.; Shi, S.; Wang, B. K.; Jalan, A. A.; Kang, M. K.; Wickremasinghe, N. C.; Hartgerink, J. D. Highly Angiogenic Peptide Nanofibers. *ACS Nano* **2015**, *9*, 860−868.
(24) Moore, A. N.; Hartgerink, J. D. Self-Assembling Multidomain Peptide Nanofibers for Delivery of Bioactive Molecules and Tissue Regeneration. *Acc. Chem. Res.* **2017**, *50*, 714−722.
(25) Lin, Y.-A.; Cheetham, A. G.; Zhang, P.; Ou, Y.-C.; Li, Y.; Liu, G.; Hermida-Merino, D.; Hamley, I. W.; Cui, H. Multiwalled Nanotubes Formed by Catanionic Mixtures of Drug Amphiphiles. *ACS Nano* **2014**, *8*, 12690−12700.
(26) Raymond, D. M.; Nilsson, B. L. Multicomponent Peptide Assemblies. *Chem. Soc. Rev.* **2018**, *47*, 3659−3720.
(27) Du, X.; Zhou, J.; Shi, J.; Xu, B. Supramolecular Hydrogelators and Hydrogels: From Soft Matter to Molecular Biomaterials. *Chem. Rev.* **2015**, *115*, 13165−13307.
(28) Acar, H.; Srivastava, S.; Chung, E. J.; Schnorenberg, M. R.; Barrett, J. C.; LaBelle, J. L.; Tirrell, M. Self-Assembling Peptide-Based Building Blocks in Medical Applications. *Adv. Drug Delivery Rev.* **2017**, *110−111*, 65−79.
(29) Adler-Abramovich, L.; Gazit, E. The Physical Properties of Supramolecular Peptide Assemblies: From Building Block Association to Technological Applications. *Chem. Soc. Rev.* **2014**, *43*, 6881−6893.
(30) Fleming, S.; Ulijn, R. V. Design of Nanostructures Based on Aromatic Peptide Amphiphiles. *Chem. Soc. Rev.* **2014**, *43*, 8150−8177.
(31) San, B. H.; Hwang, J.; Sampath, S.; Li, Y.; Bennink, L. L.; Yu, S. M. Self-Assembled Water-Soluble Nanofibers Displaying Collagen Hybridizing Peptides. *J. Am. Chem. Soc.* **2017**, *139*, 16640−16649.
(32) Yang, S.; Dong, H. Modular Design and Self-Assembly of Multidomain Peptides Towards Cytocompatible Supramolecular Cell Penetrating Nanofibers. *RSC Adv.* **2020**, *10*, 29469−29474.
(33) Xu, D.; Dustin, D.; Jiang, L.; Samways, D. S. K.; Dong, H. Designed Filamentous Cell Penetrating Peptides: Probing Supramolecular Structure-Dependent Membrane Activity and Transfection Efficiency. *Chem. Commun.* **2015**, *51*, 11757−11760.
(34) Xu, D.; Jiang, L.; DeRidder, L.; Elmore, B.; Bukhari, M.; Wei, Q.; Samways, D. S. K.; Dong, H. Membrane Activity of a Supramolecular Peptide-Based Chemotherapeutic Enhancer. *Mol. BioSyst.* **2016**, *12*, 2695−2699.
(35) Xu, D.; Samways, D. S. K.; Dong, H. Fabrication of Self-Assembling Nanofibers with Optimal Cell Uptake and Therapeutic Delivery Efficacy. *Bioact. Mater.* **2017**, *2*, 260−268.
(36) Xu, D.; DeRidder, L.; Elmore, B.; Dong, H. Self-Assembly of Filamentous Cell Penetrating Peptides for Gene Delivery, Peptide Self-Assembly: Methods and Protocols. *Methods Mol. Biol.* **2018**, *1777*, 271−281.
(37) Yang, S.; Xu, D.; Dong, H. Design and Fabrication of Reduction-Sensitive Cell Penetrating Nanofibers for Enhanced Drug Efficacy. *J. Mater. Chem. B* **2018**, *6*, 7179−7184.
(38) Emami, F.; Mostafavi Yazdi, S. J.; Na, D. H. Poly(lactic acid)/Poly(lactic-co-glycolic acid) Particulate Carriers for Pulmonary Drug Delivery. *J. Pharm. Invest.* **2019**, *49*, 427−442.
(39) Harush-Frenkel, O.; Bivas-Benita, M.; Nassar, T.; Springer, C.; Sherman, Y.; Avital, A.; Altschuler, Y.; Borlak, J.; Benita, S. A Safety and Tolerability Study of Differently-Charged Nanoparticles for Local Pulmonary Drug Delivery. *Toxicol. Appl. Pharmacol.* **2010**, *246*, 83−90.
(40) Menon, J. U.; Ravikumar, P.; Pise, A.; Gyawali, D.; Hsia, C. C. W.; Nguyen, K. T. Polymeric Nanoparticles for Pulmonary Protein and DNA Delivery. *Acta Biomater.* **2014**, *10*, 2643−2652.
(41) Galindo, R.; Sánchez-López, E.; Gómara, M. J.; Espina, M.; Ettcheto, M.; Cano, A.; Haro, I.; Camins, A.; García, M. L. Development of Peptide Targeted PLGA-PEGylated Nanoparticles Loading Licochalcone-A for Ocular Inflammation. *Pharmaceutics* **2022**, *14* (2), 285.
(42) Jerabek-Willemsen, M.; André, T.; Wanner, R.; Roth, H. M.; Duhr, S.; Baaske, P.; Breitsprecher, D. MicroScale Thermophoresis: Interaction Analysis and Beyond. *J. Mol. Struct.* **2014**, *1077*, 101−113.
(43) Chatterjee, A.; Mandal, D. K. Denaturant-Induced Equilibrium Unfolding of Concanavalin A is e=Expressed by a Three-State Mechanism and Provides an Estimate of its Protein Stability. *Biochim. Biophys. Acta, Proteins Proteomics* **2003**, *1648*, 174−183.
(44) Huang, Z.; Kłodzińska, S. N.; Wan, F.; Nielsen, H. M. Nanoparticle-Mediated Pulmonary Drug Delivery: State of the Art Towards Efficient Treatment of Recalcitrant Respiratory Tract Bacterial Infections. *Drug Delivery Transl. Res.* **2021**, *11*, 1634−1654.
(45) Andrade, F.; Rafael, D.; Videira, M.; Ferreira, D.; Sosnik, A.; Sarmento, B. Nanotechnology and Pulmonary Delivery to Overcome Resistance in Infectious Diseases. *Adv. Drug Deliv. Rev.* **2013**, *65*, 1816−1827.
(46) Pivard, M.; Moreau, K.; Vandenesch, F. Staphylococcus Aureus Arsenal To Conquer the Lower Respiratory Tract. *mSphere* **2021**, *6*, 000599-21.
(47) Saar, K.; Lindgren, M.; Hansen, M.; Eiríksdóttir, E.; Jiang, Y.; Rosenthal-Aizman, K.; Sassian, M.; Langel, U. Cell-Penetrating Peptides: A Comparative Membrane Toxicity Study. *Anal. Biochem.* **2005**, *345*, 55−65.
(48) Trofimenko, E.; Grasso, G.; Heulot, M.; Chevalier, N.; Deriu, M. A.; Dubuis, G.; Arribat, Y.; Serulla, M. S.; Michel, G.; Vantomme, F.; Ory, L. C.; Dam, J.; Puyal, F.; Amati, A.; Lüthi, A.; Danani, C.; Widmann, C. Genetic, Cellular, and Structural Characterization of the Membrane Potential-Dependent Cell-Penetrating Peptide Translocation Pore. *Elife* **2021**, *10*, No. e69832.
(49) Gottlieb, T. A.; Ivanov, I. E.; Adesnik, M.; Sabatini, D. D. Actin Microfilaments Play a Critical Role in Endocytosis at the Apical but Not the Basolateral Surface of Polarized Epithelial Cells. *J. Cell Biol.* **1993**, *120*, 695−710.
(50) Kuhn, D. A.; Vanhecke, D.; Michen, B.; Blank, F.; Gehr, P.; Petri-Fink, A.; Rothen-Rutishauser, B. Different Endocytotic Uptake Mechanisms for Nanoparticles in Epithelial Cells and Macrophages. *Beilstein J. Nanotechnol.* **2014**, *5*, 1625−1636.
(51) Lin, X. P.; Mintern, J. D.; Gleeson, P. A. Macropinocytosis in Different Cell Types: Similarities and Differences. *Membranes* **2020**, *10*, 177.
(52) Zanin, M.; Baviskar, P.; Webster, R.; Webby, R. The Interaction Between Respiratory Pathogens and Mucus. *Cell Host Microbe* **2016**, *19*, 159−168.
(53) Lai, S. K.; Wang, Y.-Y.; Hanes, J. Mucus-Penetrating Nanoparticles for Drug and Gene Delivery to Mucosal Tissues. *Adv. Drug Delivery Rev.* **2009**, *61*, 158−171.
(54) Hua, S.; de Matos, M. B. C.; Metselaar, J. M.; Storm, G. Current Trends and Challenges in the Clinical Translation of Nanoparticulate Nanomedicines: Pathways for Translational Development and Commercialization. *Front. Pharmacol.* **2018**, *9*, 790.
(55) Rahman Sabuj, M. Z.; Islam, N. Inhaled Antibiotic-Loaded Polymeric Nanoparticles for the Management of Lower Respiratory Tract Infections. *Nanoscale Adv.* **2021**, *3*, 4005−4018.
(56) Newman, S. P. Drug Delivery to the Lungs: Challenges and Opportunities. *Ther. Deliv.* **2017**, *8*, 647−661.
(57) Horstmann, J. C.; Thorn, C. R.; Carius, P.; Graef, F.; Murgia, X.; de Souza Carvalho-Wodarz, C.; Lehr, C.-M. A Custom-Made Device for Reproducibly Depositing Pre-Metered Doses of Nebulized Drugs on Pulmonary Cells In Vitro. *Front. Bioeng. Biotechnol.* **2021**, *9*, 643491.
(58) Messerschmidt, V. L.; Chintapula, U.; Kuriakose, A. E.; Laboy, S.; Truong, T. T. D.; Kydd, L. A.; Jaworski, J.; Pan, Z.; Sadek, H.;

https://doi.org/10.1021/acsami.2c15204
ACS Appl. Mater. Interfaces XXXX, XXX, XXX−XXX

Nguyen, K. T.; Lee, J. Notch Intracellular Domain Plasmid Delivery via Poly(Lactic-Co-Glycolic Acid) Nanoparticles to Upregulate Notch Pathway Molecules. *Front. Cardiovasc. Med.* **2021**, *8*, 707897.

(59) Iyer, R.; Nguyen, T.; Padanilam, D.; Xu, C.; Saha, D.; Nguyen, K. T.; Hong, Y. Glutathione-Responsive Biodegradable Polyurethane Nanoparticles for Lung Cancer Treatment. *J. Controlled Release* **2020**, *321*, 363−371.

(60) Casciaro, B.; d'Angelo, I.; Zhang, X.; Loffredo, M. R.; Conte, G.; Cappiello, F.; Quaglia, F.; Di, Y.-P. P.; Ungaro, F.; Mangoni, M. L. Poly(lactide-co-glycolide) Nanoparticles for Prolonged Therapeutic Efficacy of Esculentin-1a-Derived Antimicrobial Peptides Against Pseudomonas Aeruginosa Lung Infection: In Vitro and In Vivo Studies. *Biomacromolecules* **2019**, *20*, 1876−1888.

https://doi.org/10.1021/acsami.2c15204
ACS Appl. Mater. Interfaces XXXX, XXX, XXX−XXX